PAIR PLASMAS IN THE CENTRAL ENGINE OF ACTIVE GALACTIC NUCLEI

S. Tsuruta & B.G. Tritz

Department of Physics, Montana State University

ABSTRACT

As the most promising model for the X-ray emission from a class of active galactic nuclei (AGNs) represented by radio-quiet quasars and Seyfert nuclei, here we introduce the non-thermal pair cascade model, where soft photons are Comptonized by non-thermal electron-positron pair plasmas produced by γ-rays. After summarizing the simplest model of this kind, the "homogeneous spherical cascade model", our most recent work on the "surface cascade model" is presented, where a geometrical effect is introduced. Many characteristics of this model are qualitatively similar to the homogeneous cascade model. However, an important difference is that γ-ray depletion is much more efficient in the surface cascade, and consequently this model naturally satisfies the severe observational constraint imposed by the γ-ray background radiation.

1. INTRODUCTION

Until relatively recently the X-ray spectrum from AGNs was thought to be a rather featureless power-law which could be explained by a variety of physical models, and hence it was difficult to distinguish one model from another (e.g. Ref. 1). During the last several years at least for a class of AGNs represented mostly by Seyfert nuclei and radio-quiet quasars, this situation has changed dramatically, due to instrumental advances in such satellite missions as EXOSAT, Ginga, and ROSAT. Data for these AGNs from EXOSAT and Ginga clearly showed that several interesting features, such as the soft X-ray excess, an iron line-edge feature, and hard X-ray hump, are superimposed on the generally power-law X-ray spectrum (e.g. Refs. 2,3,4). It is generally thought that radio-quiet quasars and Seyfert nuclei are powered by accretion of gas onto a supermassive black hole (e.g. Refs. 1,5). Then, the presence of relatively cool, dense plasmas is inevitable near the central engine of these objects (Ref. 6). Consequently, even before its discovery the presence of these additional fine features has been predicted as a natural consequence of the reprocessing of X-rays by these cool plasmas in the central engine (Refs. 6,7).

Among various models suggested for the roughly power-law X-ray spectrum from this type of AGNs, the most promising appears to be the Comptonization of soft photons by energetic electrons, produced either thermally or non-thermally (e.g. Refs. 8,9). We shall briefly explain why electron-positron (e^- - e^+) pairs may be important in this type of models. Accepting the supermassive black hole model where accretion to the hole is responsible for the power supply, the temperature of protons in the accreting plasmas will reach $\sim 10^{12}$ K if all the released gravitational energy is used to heat the gas. Even if only the Coulomb interaction is considered electrons will be heated to $\sim 10^9$ K, with the thermal energy close to the rest mass energy. If more efficient proton-electron interaction mechanisms are in operation (e.g. some collective plasma processes (Ref. 10)) the electron temperature may become higher. Then production of e^- - e^+ pairs will be inevitable. It has been pointed out, on the other hand, that in the environment of the innermost portion of accretion flows in the central engine of AGNs, the accretion energy could be radiated non-thermally, e.g. by accelerating some fraction of electrons to highly relativistic energies. These electrons will emit gamma rays, which will produce e^- - e^+ pairs before escaping the system if it is sufficiently compact (e.g. Ref. 9).

Non-thermal injection of relativistic electrons is more efficient than thermal production. Also the observed detailed spectral and temporal behaviour appears to favour the non-thermal model. For instance, in the thermal Compton model soft photons are up-scattered by thermal electrons (and pairs) to produce the observed X-ray power-law spectrum, and hence harder X-ray variations should lag the softer variations. On the other hand, the observed behaviour is far more complicated. For instance, the hard lags the soft in some sources, but the reverse is seen in some other sources. Such complicated behaviour is predicted from the non-thermal Compton model, where the direction of the lags depends on various different physical conditions, e.g. the fraction of the input energy channeled into relativistic electron injection. Consequently, the physical mechanism most extensively explored theoretically has been the non-thermal process (Refs. 9,11-14).

Proceedings of the Fourth International Conference on Plasma Physics and Controlled Nuclear Fusion, held in Toki, Japan, 17–20 November 1992 (ESA SP-351, February 1993).

2. HOMOGENEOUS SPHERICAL CASCADE MODEL

In the simplest kind of the non-thermal Compton model, blackbody soft photons are up-scattered by relativistic electrons injected with a high Lorentz factor. Relativistic electrons will emit gamma rays which will produce the e^- - e^+ pairs through photon-photon collisions before escape and the process will continue in cascade, if the source is sufficiently compact (Refs. 11-14). We shall refer to this type of model the "non-thermal pair cascade model". It has been shown that the presence of the soft photon source, however, is not required for this type of cascade process to take place. If the released accretion energy is used 100% to accelerate electrons to a high Lorentz factor and to emit synchrotron radiation in a highly compact object, the gamma ray end of the synchrotron photons will produce e^- - e^+ pairs which will up-scatter the lower energy portion of the same radiation, and the process will continue in cascade (Ref. 9). The result is the steepening of the primary synchrotron radiation and the depletion of the gamma ray end of the radiation. In the more recent calculations, therefore, it has been a standard practice to keep as a free parameter the ratio of the fraction of the input energy channeled into the hard component (relativistic electrons) to the fraction in the soft component (soft photons) (Refs. 11-14).

The compactness of AGNs is considered to be very high (e.g. Ref. 14). This is due to the very short timescale of large amplitude X-ray variability detected from many of these objects, for instance, 300 to 1000 secs in Seyfert nuclei such as NGC 6814, NGC 4051 and MCG 6-30-15. Accepting the cosmological redshift, the typical luminosity of AGNs is $\sim 10^{41}$ - 10^{48} ergs sec^{-1}. For such highly luminous objects the central black hole mass is required to be $\sim 10^6$ - 10^8 $M_\odot$ (e.g. Refs. 1,5). Then the X-ray emission region will be typically ~ 10 R_g (where R_g is the gravitational radius of the black hole).

The non-thermal pair cascade model investigated earlier has been confined to a homogeneous spherical case where soft and hard injection, and the resulting electron-positron pair plasma, are uniformly distributed within a spherical region. We shall refer to this model the "homogeneous spherical cascade model".

2.1 Methods

Plausible primary emission spectra are constructed generally by drawing upon theory and observation. In a wide class of radio-quiet quasars and luminous Seyfert nuclei there exists a prominent feature in the hard UV, the "UV bump", which rises above the extrapolated power-law of the energy index ~ 1. The most recent ROSAT results show that all Seyfert nuclei observed have the X-ray soft excess, and moreover the soft excess and the UV bump variations are strongly correlated (Trümper, private communication). Therefore, it is most likely that the UV bump extends to the soft X-ray region, and this UV to soft X-ray thermal emission is the peak of a multiple temperature, quasi-blackbody spectrum from cool (10^4 - 10^5 K) gas, existing as cool clouds within hotter plasma or as an accretion disk. The model, therefore, generally includes a "soft" component of the primary spectrum, given by the specific flux distribution $F_s(x)$ (erg cm^{-2} sec^{-1} per unit x), which is proportional to a Planck distribution at temperature T_d, where $x = h\nu/m_ec^2$. A characteristic soft energy $x_s = 2.8\ kT_d/(m_ec^2)$ is defined at the peak of the soft emission. The compactness parameter corresponding to soft emission is defined by $l_s = L_s\sigma_T/(Rm_ec^3)$, where $L_s = 4\pi R^2 \int F_s(x)dx$ is the soft luminosity and σ_T is the Thomson cross section.

For substantial pair production to occur, a sufficiently strong flux of hard ($x > \sim 1$) photons must be present. Various authors have argued that accretion flows are natural sites for γ-ray production, through the presence of one or more particle acceleration mechanisms, such as shocks, magnetic reconnection, etc. Although it is difficult to make specific quantitative calculations of such systems, it has been found that these relativistic particle accelerations generally produce power-law radiation (e.g. Refs. 9,11-14). Therefore, a "hard" primary spectral component, $F_h(x)$, is generally modeled as a power-law, with spectral index α_0, and extending from the soft energy x_s to a maximum emitted energy x_m. The compactness associated with hard emission is defined as $l_h = L_h\sigma_T/(Rm_ec^3)$, where $L_h = 4\pi R^2 \int F_h(x)dx$ is the hard luminosity. The relative strength of the soft and hard emission is set by the model parameter l_s/l_h, which is the ratio of soft to hard compactness (or the ratio of soft to hard luminosity, since both are emitted from the same source). The total compactness of the source is $l = L\sigma_T/(Rm_ec^3)$, where $l = l_s + l_h$ and $L = L_s + L_h$ is the total luminosity. Further details on the equations and methods are found in Refs. 11-14.

2.2 Results and Discussion

The detailed behaviour of the homogeneous spherical cascade model has been investigated using various different injection parameters (Refs. 11-14). The dotted curves in Figure 1 show, for the homogeneous spherical cascade model, the emergent spectra from representative models with the following injection parameters: $x_s = 3 \times 10^{-5}$, $l_s/l_h = 0.25$, $x_m = \sim 5 \times 10^3$, $\alpha_0 = 0.5$, and $l_h = \{1, 10, 100, 1000\}$. The effect of varying the hard compactness l_h is clearly seen. Increasing l_h leads to increases in pair yield, thermal pair optical depth, and annihilation line strength. Depletion and steepening of the γ-ray spectrum occurs as more high energy photons are absorbed in pair creation, initially at x_m and proceeding down towards $x \approx 1$ with increasing compactness. Enhancement of the x-ray spectrum occurs as γ-rays are reprocessed through pairs and reappear at X-ray energies. The X-ray energy index α_x steepens from 0.5 (the injected photon index corresponding to monoenergetic particle injection) towards 1.0, the final value depending principally upon the number of pair generations produced. See Refs. 11-14 for further details.

This model naturally explains many aspects of the observed spectrum, such as the presence of the UV bump, soft X-ray excess, and a medium-to-hard X-ray energy index confined to ~ 0.5 - 1. However, this model poses a serious problem in the sense that the high energy tail of the emergent spectrum exceeds the constraint imposed by the γ-ray background radiation, unless a very limited fine tuning of model parameters is imposed (Refs. 12,14).

3. SURFACE CASCADE MODEL

Very recently a possible geometrical effect is introduced, for the first time, in the calculations of the non-thermal pair cascade model (Refs. 15,16). In this model hard and soft photon injection are no longer distributed throughout the pair

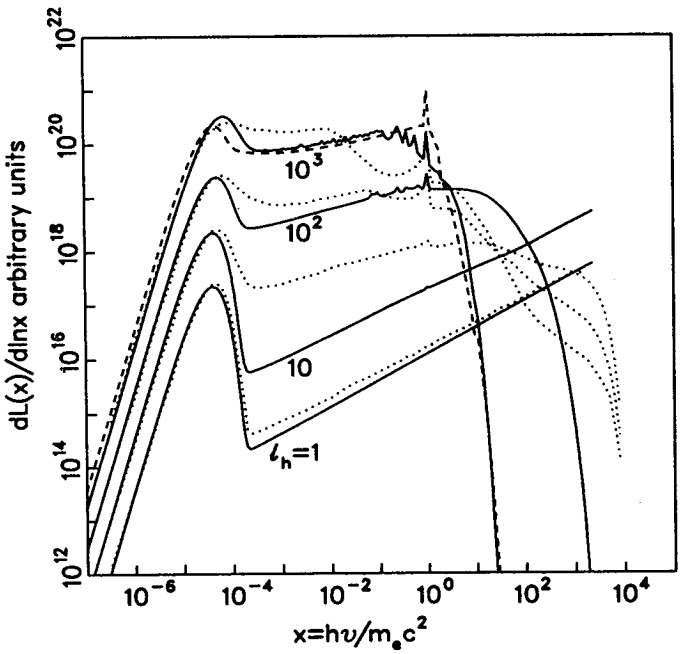

Fig. 1: Emergent spectra for primary thermal soft photon and power-law hard photon injection, with $x_s = 3 \times 10^{-5}$, $x_m = \sim 5 \times 10^3$, $l_s/l_h = 0.25$, $\alpha_0 = 0.5$, and $l_h = \{1, 10, 100, 1000\}$. The solid curves show the surface cascade model, while the dotted curves refer to the homogeneous spherical cascade model. The dashed curve shows the surface cascade model with $l_h = 1000$ when scattering by thermal pairs is neglected.

plasma, but are concentrated along the source surface. Specifically, a spherical or planar surface source emits soft photons and γ-rays, which initiate a pair cascade in the space surrounding the source, producing a pair atmosphere or corona above the surface. We shall refer to this model the "surface cascade model". Detailed, self-consistent calculations were carried out for the structure of the resulting pair-photon atmosphere and of the spectral reprocessing which occurs (Refs. 15,16).

3.1 Methods

Various elements of a set of the adopted equations and methods are taken from previous cascade calculations (Refs. 12,13,14), as briefly summarized in Section 2.1. However, we replace equations describing radiative transfer in a homogeneous spherical system by those corresponding to radial out-streaming of radiation from the source in the surface cascade. The computer code was constructed such as to accept arbitrary primary spectra within the range of dimensionless photon energies $10^{-8} < x < 2 \times 10^4$. However, in the results shown below the same primary spectrum as specified in Section 2.1 is used at the source.

3.2 Results and Discussion

Solid curves in Figure 1 show, for the surface cascade model, the emergent spectra from models with the same injection parameters as in the homogeneous model shown in Section 2.2 (dotted curves): $x_s = 3 \times 10^{-5}$, $l_s/l_h = 0.25$, $x_m = \sim 5 \times 10^3$, $\alpha_0 = 0.5$, and $l_h = \{1, 10, 100, 1000\}$. The non-zero annihilation line widths result from the finite energy resolution used in the calculations. The secondary peaks softward of the annihilation feature result from the approximate treatment of thermal Comptonization, specifically from the neglect of dispersion and from the absence of separate treatment for scattering the annihilation line.

Much of the spectral behaviour noted in Refs. 11-14 for homogeneous spherical injection is seen in the surface cascade results as well, with the important exception of enhanced depletion at the highest γ-ray energies in the surface cascade. For instance, the effect of varying the hard compactness l_h, as noted in Section 2.2, is clearly seen. Here little spectral evolution is seen for $l_h << \sim 160$ (i.e., the $l_h = 1$ and 10 curves in Figures 1), while substantial reprocessing occurs for $l_h >> \sim 160$ (i.e., the $l_h = 1000$ curve). The effect of scattering by thermal pairs is seen in Figure 1, where the dashed curve indicates $l_h = 1000$ without thermal Comptonization. Thermal pairs downscatter photons from the energy range $1/(\tau_T)^2 \leq x \leq 1$, depleting this region, as can be seen in the spectra. Here, τ_T is the optical depth of the atmosphere in thermal electrons and positrons. Thermal upscattering of the soft blackbody source is readily seen in Figure 1, but the scattered peak is not nearly as broadened as in the homogeneous model (dotted curves), due in part to the lack of dispersion in our treatment of thermal scattering.

A comparison of the γ-ray region in the surface cascade model (solid curves) with the homogeneous case (dotted

curves) illustrates an important difference between these two cascade models. While there is seen a progressive depletion and steepening of the γ-ray spectrum with increasing l_h in both models, in surface cascades the depletion is more pronounced; indeed, a progressively complete emptying of the γ-ray spectrum starts at l_h significantly lower than in the homogeneous case. This enhanced depletion is a direct result of the surface cascade geometry, in which γ-rays must travel through the entire column of absorbing atmosphere lying above their point of injection or creation and extending out to around the freeze-out radius at $h \approx R$, before becoming part of the emergent spectrum. In contrast, γ-radiation injected or created within absorption optical depth unity of the surface of a homogeneous spherical injection region is more or less free to escape. For large hard compactness the optical depth can be quite large, and the exponential depletion in the surface cascade may far outstrip the much weaker depletion in the homogeneous model. Further details are found in Ref. 15.

To obtain the surface cascade results shown in Figure 1 (solid and dashed curves) our attention was restricted to a specific type of atmosphere, the pair cascade shower, in which scattering of radiation back down towards the accretion flow is neglected. This and some other simpler assumptions were relaxed in Ref. 16, where the general case of arbitrarily anisotropic atmospheres is investigated. However, we have found that the surface cascade results presented in Figure 1 agree qualitatively with the more exact results of Ref. 16. In view of the excessive computing requirements needed for the exact approach and its practical usefulness, we conclude that the surface cascade results shown in Figure 1 are justified.

The surface cascade results shown in Figure 1 were also obtained by adopting a spherical geometry, with the source radius R. Tritz (Ref. 16) investigated uniform, infinite planar sources and obtained results that are qualitatively similar to Figure 1, if a cutoff height is imposed on spectral evolution above the planar source. The location of such a cutoff is somewhat arbitrary, requiring the specification of an additional model parameter. Spherical models, however, are more physical in the sense that the $n \sim r^{-2}$ density dilution will effectively terminate spectral evolution in the vicinity of the "freeze-out" height at $h \sim R$. Because the surface pair cascade is limited to the space immediately surrounding the source (see Refs. 15,16), the results from the spherical source should be applicable to the planar geometry of a disk corona model, if a suitable cutoff is imposed.

3.3 Comparison with Observation

In order to delineate a parameter space in which the surface cascade model is consistent with observations, the approach of Ref. 14 was adopted and the following constraints were applied to the model. The first constraint is that many AGNs exhibit a 2 - 10 keV spectral energy index in the range $0.6 < \alpha_x < 0.9$, with a mean value around 0.7 (Refs. 12,14). The emergent X-ray energy index α_x was calculated from the slope of a power law fit to this energy band. Second, the ratio of UV luminosity to X-ray luminosity, l_s/l_x, is observationally restricted to the range $1 < l_s/l_x < 10$ (refs. 12,14). Here l_s is a model parameter and l_x is obtained by integrating energy flux over 2 - 10 keV. Third, observations of the γ-ray background provide an upper limit to the strength of the 1 - 100 MeV band for a given 2 - 10 keV flux (Refs. 12,14). The γ-ray excess is defined as the ratio of the calculated 1 - 100 MeV energy flux to the maximal value allowed by the observed γ-ray background radiation (Ref. 14). To be consistent with the γ-ray background measurements, AGNs in general must exhibit excesses less than or equal to unity. The fourth constraint is a maximum strength of the annihilation line required by the failure to detect the feature in observed spectra (Ref. 14). Line strength is measured in terms of its equivalent width, EW (keV), which is the ratio of annihilation photon flux density to continuum photon flux density at the line energy. If it is assumed that turbulent velocities in the system reach 0.3 c (a reasonable value as argued in Ref. 14), then annihilation lines must have EW < 300 keV to remain undetected. The continuum flux density is calculated by interpolation on a power-law fit between x = 0.3 and x = 3.0 (Ref. 14).

We have calculated α_x, l_s/l_x, the γ-ray excess, and the equivalent width of the annihilation line for models whose injection parameters are chosen to allow direct comparison with results in Ref. 14. Specifically, we have chosen two typical cases. Model (a) represents a relatively high energy injection which is capable of producing several generations of pairs: $x_s = 10^{-4}$, $x_m = 1.333 \times 10^4$, $\alpha_0 = 0.5$, $l_s/l_x = \{10, 1, 10^{-1}, 10^{-2}\}$, and $7 \times 10^{-2} \leq l_h \leq 7 \times 10^3$. Model (b) represents a low energy injection which is capable of producing one generation of pairs: $x_s = 10^{-5}$, $x_m = 13.33$, $\alpha_0 = 0.5$, $l_s/l_x = \{10, 1, 10^{-1}, 10^{-2}\}$, and $7 \times 10^{-2} \leq l_h \leq 7 \times 10^3$. We find that successful models, consistent with all constraints, are produced by a moderately wide range of injection parameters. For the high energy model (a) the approximate criteria are $\sim 0.1 < l_s/l_h < \sim 1.0$ and $\sim 120 < l_h < \sim 5800$, while for the low energy model (b) they are $\sim 0.1 < l_s/l_h < \sim 0.5$ and $\sim 310 < l_h < \sim 4300$. These criteria are sufficiently similar that the following general criteria to meet observational constraints for either case may be stated: $\sim 0.1 < l_s/l_h < \sim 0.7$ and $\sim 200 < l_h < \sim 5000$ (Ref. 15). In contrast, Done and Fabian (Ref. 14) find that no homogeneous spherical injection model robustly satisfies all constraints, and that only a narrow range of parameter values will marginally satisfy them.

4. SUMMARY AND CONCLUDING REMARKS

As the promising model of a class of AGNs represented by radio-quiet quasars and Seyfert nuclei the non-thermal pair cascade model is introduced. After presenting the simplest model of this kind, the homogeneous spherical cascade model, the surface cascade model is introduced where a possible geometrical effect is included. Here the source of soft photons and γ-rays are concentrated along the surface of a sphere of radius R, and the pair cascade takes place in the coronal region above the source. Various characteristics of the results are qualitatively similar to those exhibited by the homogeneous spherical model in which photon and particle injection and the pair cascade are uniformly distributed throughout a spherical region. However, by geometrically separating injection from the pair cascade, we obtained an important, qualitatively different result.

A major problem of the homogeneous pair cascade model is the production of a high energy tail excess, above the severe constraint imposed by the γ-ray background radiation (Refs. 12,14), unless model parameters are very finely tuned. This high energy excess, however, no longer appears in the surface cascade model, for a wide range of injection parameters. This is due to the more efficient depletion of γ-

rays. In this way the γ-ray excess problem is naturally solved in the surface cascade model. In particular, we find that the observational constraints on the X-ray spectral index, the ratio of soft to hard luminosity, the annihilation line strength and the γ-ray excess are satisfied by a wide range of typical injection parameters, with $\sim 0.1 < l_s/l_h < \sim 0.7$ and $\sim 200 < l_h < \sim 5000$. Similar results were obtained when a planar (instead of a spherical) geometry is adopted for the source distribution, if an appropriate cutoff height is imposed (Ref. 16), and hence this model is applicable to a disk corona configuration, too.

The surface cascade model presented here examines the Comptonization of soft photons, emitted by an accretion flow, by the electron-positron pair plasma created in the region above the flow. We have neglected an important reverse process, of further reprocessing of the X-ray power-law emission by the cooler gas in the accretion flow, which is responsible for the production of additional fine spectral features such as the iron line-edge structure and hard X-ray hump. Ideally, these two-way processes should be solved simultaneously, and this more realistic case will be treated in our future work.

ACKNOWLEDGEMENTS

We acknowledge with thanks useful discussions with M.J. Rees, A. Fabian, Y. Uchida, Lightman, R. Svensson and M. Begelman. This work was supported in part by the NASA grant NAGW-2208 and NSF grant RII-8921978.

REFERENCES

1. Rees MJ 1984, Ann. Rev. Astr. Ap., 22, 471 p.

2. Nandra K & al 1991, M.N.R.A.S., 248, 760 p.

3. Pounds KA & al 1989, M.N.R.A.S., 240, 769 p.

4. Matsuoka M & al 1990, Ap. J., 361, 440 p.

5. Blandford RD 1985, Proceedings of Manchester Conference on AGN, Manchester, UK.

6. Guilbert PW & Rees MJ 1988, M.N.R.A.S., 233, 475 p.

7. Lightman AP & White TR 1988, Ap.J., 335, 57 p.

8. Takahara F & Tsuruta S 1982, Progr.Theoret.Phys., 67, 485 p.

9. Guilbert PW, Fabian AC, & Rees MJ 1983, M.N.R.A.S., 205, 593 p.

10. Begelman MC & Chiueh T 1988, Ap.J., 332, 872 p.

11. Fabian AC & al 1986, M.N.R.A.S., 221, 931 p.

12. Lightman AP & Zdziarski AA 1987, Ap.J., 319, 643 p.

13. Svensson R 1987, M.N.R.A.S., 227, 403 p.

14. Done C & Fabian AC 1989, M.N.R.A.S., 240, 81 p.

15. Tritz BG & Tsuruta S 1992, submitted to Ap.J.

16. Tritz BG 1990, Ph.D. Thesis, Montana State University.